Target diagnostic system for the national ignition facility (invited)

R. J. Leeper, G. A. Chandler, G. W. Cooper, M. S. Derzon, D. L. Fehl, D. E. Hebron, A. R. Moats, D. D. Noack, J. L. Porter, L. E. Ruggles, C. L. Ruiz, and J. A. Torres
Sandia National Laboratories, Albuquerque, New Mexico 87185

M. D. Cable, P. M. Bell, C. A. Clower, B. A. Hammel, D. H. Kalantar, V. P. Karpenko, R. L. Kauffman, J. D. Kilkenny, F. D. Lee, R. A. Lerche, B. J. MacGowan, M. J. Moran, M. B. Nelson, W. Olson, T. J. Orzechowski, T. W. Phillips, D. Ress, G. L. Tietbohl, and J. E. Trebes
Lawrence Livermore National Laboratory, Livermore, California 94550

R. J. Bartlett, R. Berggren, S. E. Caldwell, R. E. Chrien, B. H. Failor, J. C. Fernandez, A. Hauer, G. Idzorek, R. G. Hockaday, T. J. Murphy, J. Oertel, R. Watt, and M. Wilke
Los Alamos National Laboratory, Los Alamos, New Mexico 87545

D. K. Bradley and J. Knauer
University of Rochester, Rochester, New York 14627

R. D. Petrasso and C. K. Li
Massachusetts Institute of Technology, Plasma Fusion Center, Cambridge, Massachusetts 02139

(Presented on 15 May 1996)

A review of recent progress on the design of a diagnostic system proposed for ignition target experiments on the National Ignition Facility (NIF) will be presented. This diagnostic package contains an extensive suite of optical, x ray, gamma ray, and neutron diagnostics that enable measurements of the performance of both direct and indirect driven NIF targets. The philosophy used in designing all of the diagnostics in the set has emphasized redundant and independent measurement of fundamental physical quantities relevant to the operation of the NIF target. A unique feature of these diagnostics is that they are being designed to be capable of operating in the high radiation, electromagnetic pulse, and debris backgrounds expected on the NIF facility. The diagnostic system proposed can be categorized into three broad areas: laser characterization, hohlraum characterization, and capsule performance diagnostics. The operating principles of a representative instrument from each class of diagnostic employed in this package will be summarized and illustrated with data obtained in recent prototype diagnostic tests. © *1997 American Institute of Physics.* [S0034-6748(97)69001-2]

I. INTRODUCTION

The National Ignition Facility (NIF) is a glass laser which will initially be used to demonstrate ignition and gain in an inertially confined plasma. The proposed facility will use modern electro-optic technology, compact segmented amplifiers, and multipass laser architecture. Improvements in optical manufacturing will enable optical fluences greater than 2 to 4 times those used on the Nova facility, substantially reducing the total laser aperture (and thus costs) required for ignition performance. Figure 1 is a schematic of the NIF from the recently completed conceptual design report. The facility will be operated by the Department of Energy (DOE). Preliminary engineering design of the facility has now been completed.

The NIF, as currently proposed, is a 192 beam, frequency-tripled ($\lambda = 0.35\ \mu$m) Nd:glass laser system with routine on-target energy and power of 1.8 MJ and 500 TW, appropriately pulse shaped. A scientific prototype of one of the NIF beams, the ''Beamlet,'' is operational and has demonstrated most of the NIF laser requirements, including laser fluence and high-efficiency conversion to 0.35 μm light. The Beamlet will be used to continue to refine the NIF laser design before construction is initiated.

The NIF system design requirements given in Table I for indirect drive have been determined from the baseline hohlraum and capsule target shown in Fig. 2.[1] The hohlraum in Fig. 2 uses 1.35 MJ of absorbed energy to drive the 150 kJ capsule at 300 eV. The light entering each laser entrance hole (LEH) in Fig. 2 is in two cones, so that it is possible to minimize the time-dependent asymmetry in the x rays incident on the capsule by dynamically varying the relative brightness of the cones. About a third of the energy must go into the cones near the target midplane. The 192 beams are clustered in groups of 4, so that there are effectively 8 spots in each of the inner cones, and 16 in the outer cones. Each cluster of four beams combine to form an effective $f/8$ optic.

Although indirect drive is the primary approach to ignition on the NIF, developments in direct drive have reached the point where this approach also looks quite promising. With the implementation of additional beam smoothing and more beam ports on the target chamber, the NIF can be configured to be capable of both indirect and direct drive. The target chamber and diagnostics are being designed to not preclude direct drive targets.

A preliminary experimental plan for the ignition activities of the facility has been prepared. This experimental plan

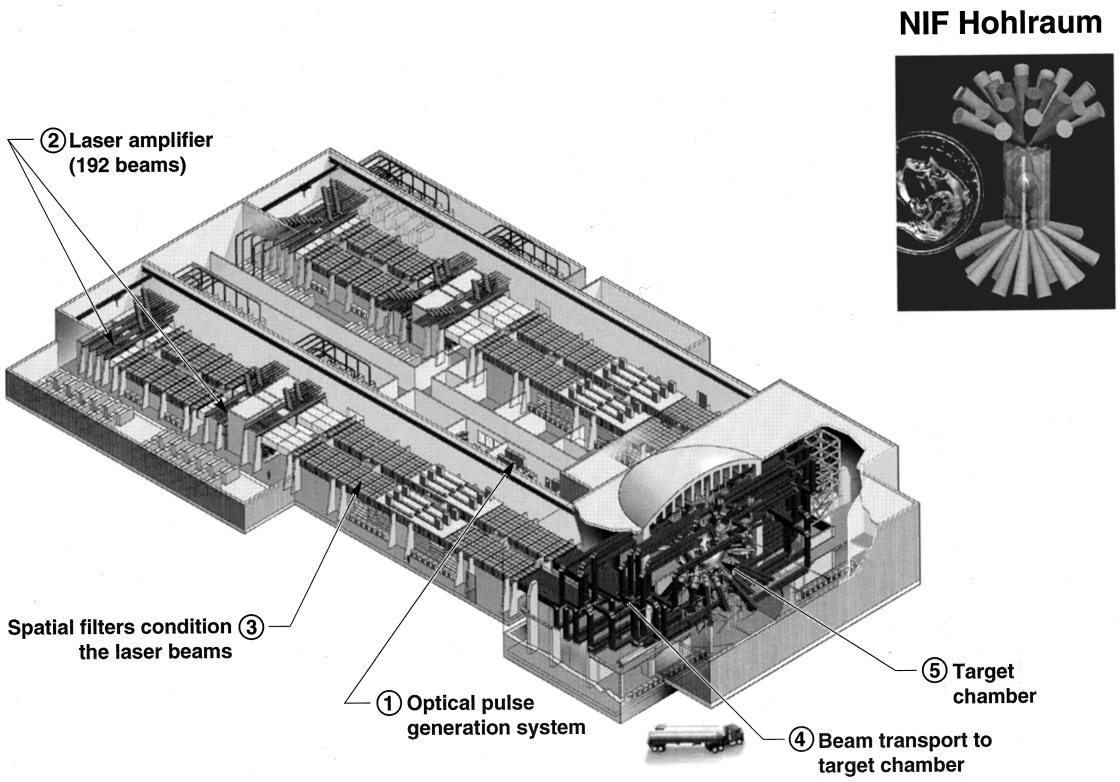

FIG. 1. Overall layout of the NIF facility showing the U shape.

has determined the target chamber layout and the initial diagnostics required for the facility to achieve its near term mission of ignition and gain. The diagnostics required for laser activation, hohlraum tuning, and initial implosion physics experiments have been conceptually designed. Prototype testing of many of these diagnostics has now been started. Diagnostics required for later implosion experiments have been considered in so far as they impact the layout of the target chamber and the target area.

The overall concept for the target area facility is a laser system that is ''*U* shaped'' in plan, as shown in Fig. 1. The target chamber is housed in a 30.5 m diam by 29.3-m-tall, reinforced concrete building. The NIF baseline design target chamber is a 10-cm-thick by 10 m internal diameter, spherical aluminum shell. The aluminum wall provides the vacuum barrier and mounting surface for the first wall protective shield panels. These boron carbide wall panels provide a protective layer from soft x rays and shrapnel. A backlighter capability can be obtained by diverting some of the beams to a focal spot that is up to 5 cm from the center of the chamber. The 192 beams enter target chamber ports located in four circular configurations defined by the intersection of cones with 27 and 52 deg polar angles. Lenses with f-number 22, in clusters of four, are positioned 7 m from chamber center to create laser focal spots of 500 μm diam at the entrance to the target hohlraum.

The startup and laser validation portion of the NIF experimental plan will require time- and space-resolved x-ray laser characterization diagnostics to synchronize the laser beams at target chamber center and confirm the pointing and focusing of the laser beams. During the hohlraum tuning portion of the experimental plan, the time history and symmetry of the x-ray drive will be measured with a set of hohlraum characterization diagnostics. During the ignition implosion physics portion of the experimental plan, a large suite of x-ray implosion physics and nuclear based capsule performance diagnostics will be employed. These three classes of diagnostics will be further categorized into ''facility-provided'' and ''experiment-specific'' diagnostics. Facility-provided diagnostics are general use target diagnostics routinely available for all NIF users. Experiment-specific diagnostics are those instruments that are designed and fielded for a particular experiment, but are not necessarily supported and made available on a routine basis. A list of the proposed current facility-provided diagnostics is given in Table II.

A top view of the NIF target chamber showing most of the facility-provided diagnostics is shown in Fig. 3. The majority of the target diagnostics are positioned around the horizontal equator of the target chamber. The diagnostic ports

TABLE I. The critical implosion parameters for ignition (NIF) implosions and the values obtained on Nova experimentally and predicted (calc.)

		Nova	
Parameter	NIF	Calc.	Expt.
Radiation temperature (eV)	300	270	270
Symmetry (%)	±0.5	±0.5	±0.5
Hohlraum plasma size (mm) (at n_e -10^{21} cm^{-3}, 3 keV)	3	3	3
Implosion velocity 10^7 cm/s	4	3.5	3.5
Hydrodynamic growth factor	400	70	60
Radial convergence	25–35	24	21
Pusher density (g/cc)	700	170	170±30

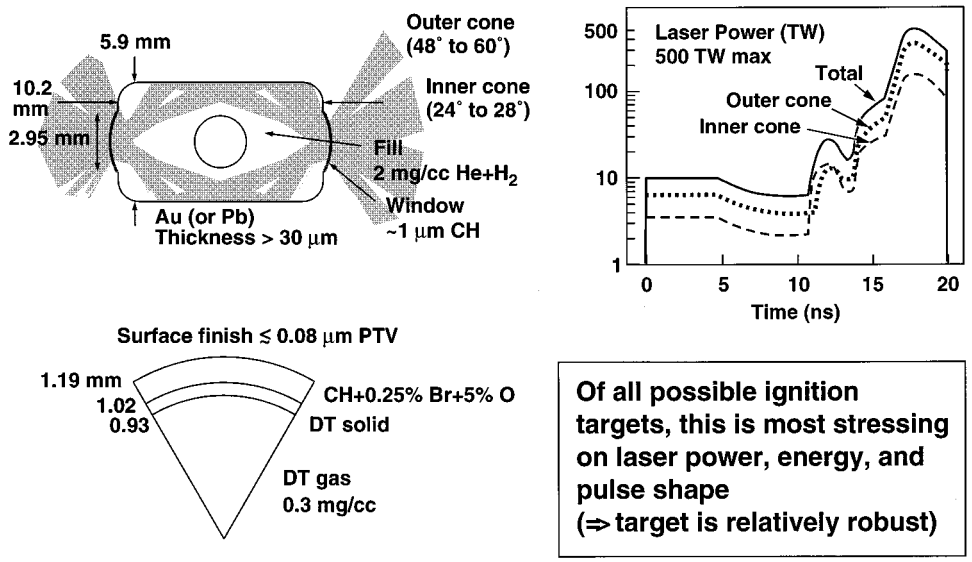

FIG. 2. A schematic of the hohlraum geometry and capsule used for high gain designs on NIF.

will accommodate many standard diagnostics, and will have a clear aperture of 45.7 cm in diameter so that experiments can use the universal, diagnostic insertion manipulators (DIMs). The DIMs provide flexibility for the rapid reconfiguration and relocation of instruments between shots. The minimum set of facility provided diagnostics have been designed and are detailed below. Many are now undergoing prototype testing. Several diagnostics that will be used after laser system validation will extend out to approximately 53 m from target chamber center (TCC), and require structural and access accommodations extending beyond the building wall. Consideration has been given to provide a flexible facility able to accommodate the entire experimental program as well as new or novel experimental designs beyond the initial phases of NIF diagnostic requirements. It is expected that eventually there will be a large number of diagnostics on the facility, similar to the 40–60 diagnostics now on Nova.[2]

A Joint Central Diagnostic Team (JCDT) has been formed that will coordinate the development of NIF diagnostics. This group, working with their home laboratories, is responsible for defining the required measurements, selecting the appropriate diagnostic techniques, developing the selected diagnostic designs, and then integrating the diagnostics into the NIF project. This group will also be responsible for defining the required diagnostic R&D program. Each laboratory will have lead primary responsibilities for a subset of the facility-provided NIF diagnostics that are funded from that laboratory's inertial confinement fusion (ICF) program funds.

II. LASER CHARACTERIZATION DIAGNOSTICS

A. Streak x-ray camera system

To measure and adjust the synchronization of the laser beams, two one-dimensional (1D) x-ray streak cameras will resolve and synchronize the x-ray emission from up to 20 laser spots focused at one time onto a target.[3] The beams need to be synchronized to ± 20 ps at the target. The diagnostic will consist of two x-ray streak cameras equipped with $2\times$ magnification slit imagers and coupled to close coupled device (CCD) readouts. The x-ray streak cameras will be housed in DIMs, which will allow their use from different viewpoints.

A 1 cm field of view in the horizontal plane at target chamber center is required to avoid overlap of emission from as many as 15 500-μm-wide laser plasmas. Imaging is required with approximately 500 μm, with temporal resolution of 10 ps resolution for x-ray energies above 2 keV. Diagnostic survivability should not be an issue, because beam synchronization will be done with a maximum of 2 kJ laser energy and a diagnostic snout at least 40 cm from target chamber center.

Synchronization targets will consist of disks of high-Z material. Front filters and the slit will be protected by a collimator to further reduce the already unlikely occurrence of debris puncturing a filter or slit substrate.

B. Static x-ray imaging system

The static x-ray imaging diagnostic (SXI) will monitor the beam pointing on all target shots.[4] Beams that miss the laser entrance hole will produce an x-ray emission spot on the hohlraum wall, indicating improper placement. This diagnostic will also be used to determine beam pointing accuracy on test targets by producing a time-integrated image of the x-ray emission produced by each laser beam irradiating the test target for 100 ps pulses.

Two SXIs will be installed near the chamber poles to image both hohlraum laser entrance holes. They will have a $2\times$ magnification, a 1 cm field-of-view, a spatial resolution of 25 μm, and will be sensitive in the 2–3 keV energy range.

The SXI consists of a sector of a Wolter grazing-incidence x-ray mirror and a flat grazing-incidence x-ray mirror. X rays emitted from the target are reflected off the flat grazing-incidence x-ray mirror to a Wolter x-ray optic consisting of a hyperboloid surface and an elliptical surface, which image the x-ray emission spot onto an x-ray CCD

TABLE II. Facility-provided NIF diagnostics.

Measurement	Diagnostic	Acronym	Lab
Laser characterization diagnostics			
Beam spot size, position, and smoothing	Static x-ray imaging system	SXI	LLNL
Beam synchronization	Streak x-ray camera system	SSC	LLNL
Energy reflected from laser plasma	Optical backscattering system	FABS	LANL/LLNL
Hohlraum characterization diagnostics			
Time history of hohlraum radiation temperature	Soft x-ray power spectral	SXSS	SNL/LANL/LLNL
Time-dependent size of hohlraum diagnostic hole; spatial symmetry of hohlraum radiation drive	Soft x-ray imaging system	SXRI	SNL
Hohlraum radiation temperature	Passive shock break-out system	SOP	LLNL
Hohlraum radiation temperature	Active shock break-out system	ASBO	SNL/LLNL
Spatial symmetry of hohlraum radiation drive	Time-resolved x-ray imaging	TRXI	LANL/LLNL/LLE
Absolute, time-integrated, high-energy hohlraum x-ray spectra	Filterfluorescer diagnostic system	FFLEX	LLNL
Capsule Characterization Diagnostics			
Capsule neutron yield	Total neutron yield system	YN	SNL/LANL
Fuel ion temperature	Neutron time-of-flight system	NTOF	LANL
Bang time and fuel burn history	Reactionn history system	RHS	LLNL/LANL
Capsule imploded core image	Neutron imaging system	NI	LLNL
Fuel areal density	Tertiary neutrons or protons	TN or TP	LLNL/LLE/MIT
Time-resolved fuel ion temperature	n-p recoil technique	TRIT	LANL/SNL

detector. Reflection angles (1°) and mirror coatings (nickel) are chosen to provide good sensitivity in the 2–3 keV x-ray region. X-ray filters such as beryllium and plastic can be used to reduce the sensitivity for cases of overlapping beams, or beams operating at very high intensities. A filter wheel will be included in each SXI to allow for rapid filter changes as necessary.

C. Optical backscatter diagnostic system

Laser energy reflected from laser produced plasmas will be measured on NIF by several optical backscatter diagnostic systems. These measurements are important to hohlraum energetics issues such as energy loss due to backscatter, electron preheat due to fast electrons from stimulated Raman scattering (SRS), and two-plasmon decay instabilities. On NIF, direct stimulated Brillouin scattering (SBS) and SRS will be measured with a full aperture backscatter station (FABS) similar to the system currently used on Nova.[5–7] This diagnostic operates by viewing the backscattered UV and visible light from the target that propagates back through the final focus lens and back down the beamline to the 1ω reflecting final turning mirror. A beam reducing telescope located behind this mirror will be used to transport the scattered light into an array of near- and far-field instrumentation packages. Instrumentation will include time-resolved imaging and spectrometry in the near and far fields and calorimetry in the SBS and SRS wavelength bands.

Backscattering measurements performed on Nova indicate that up to twice as much SBS energy may be scattered outside the final focus lens, as inside it, for gas filled targets. Because the energy outside the lens could play a large part in determining the energy budget of the interaction beam, a near backscatter imager (NBI) similar to the Nova NBI[6] is being proposed to extend the continuous coverage of SBS and SRS backscatter outside the final focusing lens acceptance angle. This diagnostic could possibly operate by imaging part of the chamber wall if scattering characteristics of wall material (or special scatter plates) was reproducible. Such a diagnostic would allow study of forward scatter from ''opposing'' beams in more open geometry experiments. The imaging cameras would separately measure SBS (near 351 nm) and SRS (400–700 nm) scattered light. Off-line calibration of the wall reflectivity, filter transmission, and TV camera sensitivity will allow the combination of the NBI images with those recorded by the FABS SBS and FABS SRS near-field cameras to provide images of the angular distribution of scatter inside and outside the interaction beam solid angle.

III. HOHLRAUM CHARACTERIZATION DIAGNOSTICS

A. Soft x-ray power diagnostic system

The soft x-ray power diagnostic (SXSS) measures the x-ray emission from a hohlraum through a lined hole in its wall, giving the time history of the radiation temperature inside the hohlraum. The diagnostic has traditionally been based on calibrated x-ray filters, mirrors, and x-ray diodes (XRDs).[8] This approach has the disadvantage of having a broad x-ray response. An alternative technique is to use a transmissive diffraction grating to disperse the x-ray flux onto an array of Si photodiode detectors.[9] A schematic of this concept is shown in Fig. 4. A system based on this technique is being tested at Sandia National Laboratories, Albuquerque. Given success in these tests, the primary NIF soft x-ray power diagnostic will be based on the transmission grating-Si photodiode technique. It may, however, be backed up by the XRD based diagnostic.

The transmission grating diagnostic, as currently envisioned, will be located entirely outside the target chamber. It uses four 5000 bar/mm, 4000-Å-thick×5-mm-tall gold transmission gratings as the spectral dispersing elements. The gratings will be located approximately 6.5 m from the center of the target chamber. A 125-μm-wide×5-mm-tall spectral slit is mounted directly in front of each grating. The spectral bandwidth of each energy channel will be varied so that each

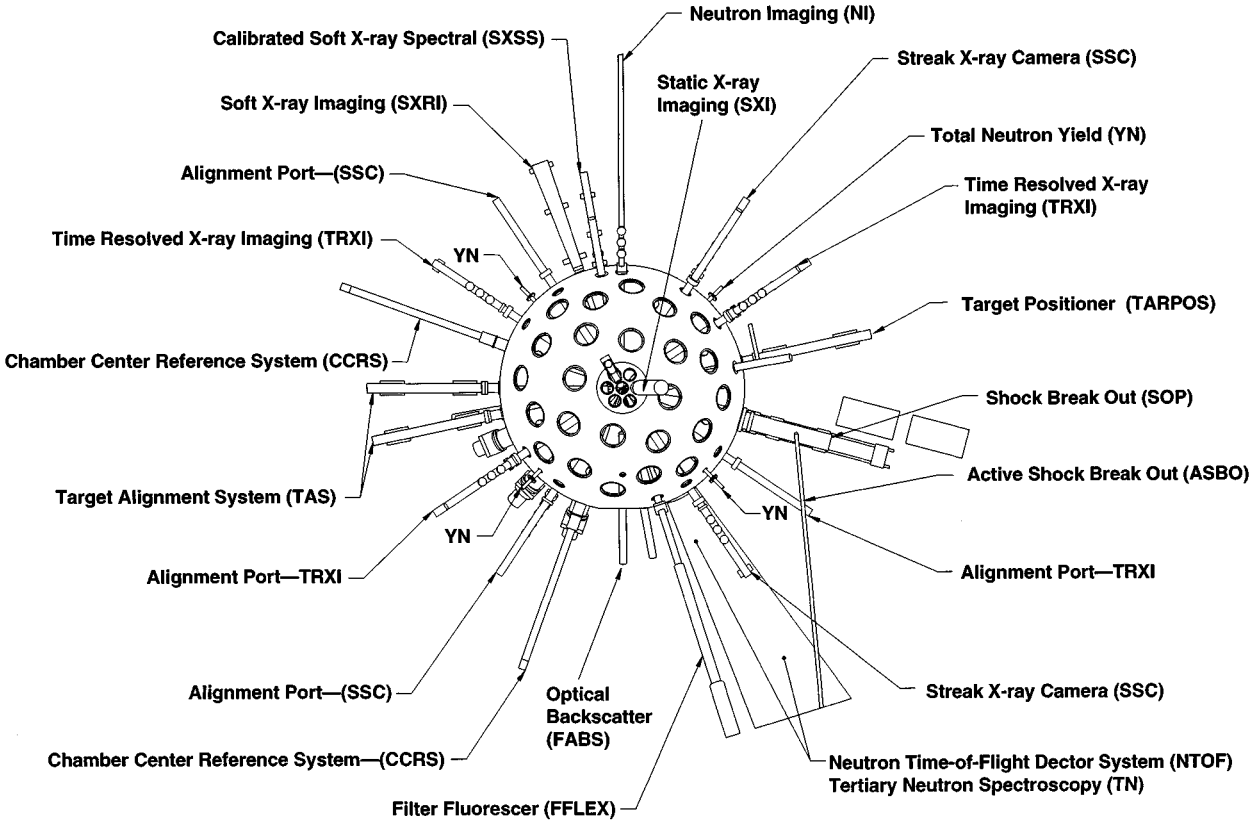

FIG. 3. A plan view of NIF target chamber showing the location of most of the target diagnostics.

channel will integrate over approximately 10% of the entire hohlraum x-ray spectrum. For this configuration, the distance between the Si photodiode detector array and the transmission grating varies between 16 mm and 1.5 m.

The diagnostic will have a total of 16 spectral channels: 8 optimized for measuring the radiation temperature during the foot of the laser pulse and 8 optimized for measuring the radiation temperature during the peak of the laser pulse.

The transmission grating diagnostic will be apertured to be blind to radiation from the region near the laser entrance holes. The diagnostic will use a 420-μm-wide$\times$5-mm-tall aperture to define the field of view of each transmission grating. This aperture will be placed approximately 1 m in front of each transmission grating. At the hohlraum wall, the full width of the umbra is 2 mm, and the full width of the penumbra is 3.4 mm.

The instrument will be protected from target debris by four pneumatically driven fast shutters located in front of each transmission grating. The shutters will close at a velocity of 75 μm/μs, closing the 125 μm slits in 2 μs. These shutters protect the instrument from target debris moving at velocities $\leqslant$300 cm/μs, expected debris velocities are $\leqslant$10 cm/μs. Radiation damage to the gratings will not be an issue for any nonigniting shots.

B. Soft x-ray imaging system

The primary mission of the soft x-ray imaging diagnostic (SXRI) is to measure the time-dependent size of the soft x-ray diagnostic hole in NIF hohlraums.[9] As a secondary mission, the SXRI will also be used to study the spatial symmetry of the radiation drive in these hohlraums. The SXRI will provide critical information, when combined with the data collected from the SXSS, to determine the time history of the NIF radiation drive. This information will make it possible to ''tune'' the NIF hohlraums and laser power to optimize the radiation field that drives NIF capsules.

The imaging system will consist of eight Cassegrain telescopes with a 1.5 X magnification. The primary mirror is concave, has a 3.26 m radius of curvature (1.63 m focal length), is 40 mm in diameter, and has an 18 mm diam through a hole in the center of the mirror. The secondary mirror is convex, has a 2.5 m radius of curvature (1.25 m focal length), and is 18 mm in diameter. The primary mirror is located 6.7 m from the center of the target chamber and is separated from the secondary mirror by 1.2 m. Four of the telescopes will use multilayer mirrors whose reflectivity is optimized at an x-ray energy of 250 eV, and four will use multilayer mirrors whose reflectivity is optimized at an x-ray energy of 500 eV. For the 250 eV mirrors, the peak reflec-

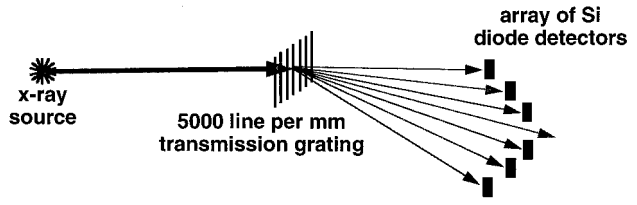

FIG. 4. A drawing of the layout of the transmission grating spectrograph.

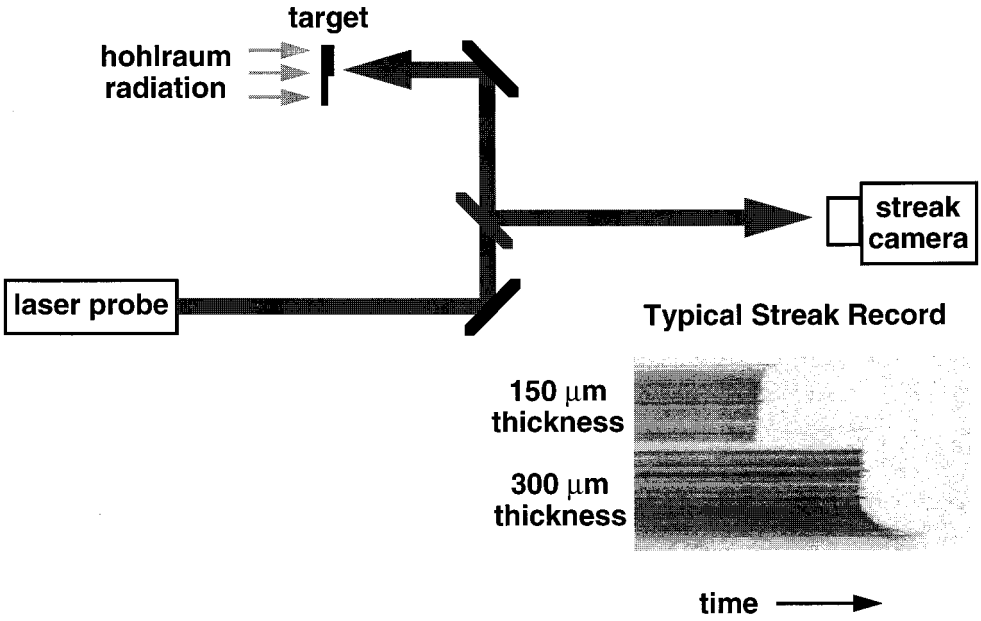

FIG. 5. A drawing showing the active shock breakout diagnostic concept and typical streaked images obtained from a 75 eV Saturn hohlraum.

tivity of each mirror at normal incidence is approximately 10%, and the bandwidth of each mirror, $\Delta E/E$, is also approximately 10%. For the 500 eV mirrors, the peak reflectivity and bandwidth of each mirror at normal incidence are approximately 1%. The diffraction-limited resolution of these telescopes, assuming perfect surfaces, is 1.0 μm at 250 eV and 0.5 μm at 500 eV. Imperfections in the mirror surfaces and misalignments of the primary and secondary mirrors will degrade this resolution.

Eight individually gateable MCP-intensified x-ray cameras with fiber-optically coupled visible CCD cameras, one for each telescope, will be used to record the x-ray images. It should be noted that the imaging system design for this diagnostic involves some technical risk for the 500 eV channel because of the difficulty in manufacturing a pair of multilayer mirrors with reflectivities at exactly the same x-ray energy to better than 1% accuracy. To achieve high precision of the central x-ray energy, these mirrors will require multilayer coating systems that are very stable. It is probable that this capability will exist in the near future.

The SXRI is located entirely outside the target chamber and will be attached to the target chamber at a vacuum port on the chamber equator close to the SXSS by means of a gimbaling mechanism. The SXRI will be supported at its far end (away from the target chamber) by a pedestal with $x-y$ positioning stages, which rests on the target area's diagnostic equatorial platform. The fragile components of the instrument will be protected from target debris by eight fast shutters, which close in 100 μs and are located in front of each of the primary mirrors of the Cassegrain telescopes.

C. Passive shock break-out system

The passive shock break-out diagnostic for NIF, also referred to as the streaked optical pyrometer (SOP), is used to determine the hohlraum temperature.[10] An equivalent instrument on Nova has been very successfully used to measure radiation temperature. X rays in the hohlraum drive a shock into a wedged witness plate. The shock velocity depends on the radiation temperature.

When the shock reaches the back of the witness plate, there is visible emission recorded by the SOP. The time difference across the wedge of the optical emission gives the shock velocity and hence the radiation temperature as interpreted through LASNEX calculations.

The Cassegrain telescope used to image the witness plate is a scaled version of the one currently in use on Nova with the same f number and magnification. The Cassegrain telescope is diffraction limited with a resolution of 7 μm and a magnification of 8.5 X for the design under consideration. The aperture of the streak camera is 40 mm. Therefore, the camera has an field-of-view of 4.7 mm, and the pointing accuracy should be better than 500 μrad in order to capture the image of the witness plate, which is 1 mm in diameter. The SOP diagnostic package is located on the equator of the NIF target chamber.

D. Active shock break-out system

The active shock break-out diagnostic (ASBO) augments the temperature range of the SOP. The ASBO uses a laser to probe the back surface of the diagnostic witness plate.[9] A low-energy, pulsed laser will illuminate the rear surface of a stepped or wedge witness plate at normal incidence. The active shock break-out diagnostic concept is illustrated in Fig. 5. The active shock break-out laser will be directed down the optical axis of the passive shock break-out diagnostic collection optics described above. The back surface of the witness plate will be polished to a mirror finish. Before the shock wave reaches the rear surface, the witness plate will reflect the laser into the passive SOP collection optics, where it will be relayed to a visible streak camera, which is coupled to a CCD. When the shock wave reaches the back surface of the witness plate, it will rapidly heat the surface,

causing the reflectivity to drop dramatically. This variant of the diagnostic may allow lower radiation temperatures to be measured. Shock pressures as low as 0.5 Mbar in aluminum targets (which corresponds to shock velocities of 0.8 cm/μs and radiation temperatures of 60–70 eV) have been measured.

The ASBO probe laser must illuminate the witness plate with an intensity significantly above the self-emission and background hohlraum-wall emission levels but below the damage threshold intensity for the witness-plate material. A bandpass filter ($\sim\pm 12.5$ nm) will be used to discriminate between the reflected laser signal and most of the background plasma emission. The self-emission level in a 25 nm bandpass for a bright shock (40 eV electron temperature) will be approximately 10^5 W/cm^2 in the visible portion of the spectrum. The probe laser will need at least a power of $\sim 10^6$ W in order to be seen over the self-emission signal, assuming that the probe laser is focused to a 3 mm diam spot on the witness plate and that all of the reflected laser light is collected by the collection optics. (The diameter of the reflected laser spot size at the SOP primary mirror will be approximately 1 cm for a laser with a 3 mr divergence.) A probe laser with an energy of $\sim$100 mJ and a pulse length of 100 ns is required to ensure that the reflected laser signal is about 10^4 times brighter than the self-emission and background-emission levels. An Alexandrite laser operating at wavelengths of 755, 390, or 255 nm has been identified as having the output characteristics needed for this diagnostic. The ASBO diagnostic is located entirely outside of the NIF target chamber.

E. Time resolved x-ray imaging system

The time-resolved x-ray imaging system (TRXI) will provide a central source of information in all phases of NIF operation. Primary requirements are for x-ray imaging in the x-ray energy range from 3 to 10 keV with a temporal resolution of 50–100 ps, similar to devices presently used on Nova that are referred to as gated x-ray imagers (GXIs).[4]

For the hohlraum symmetry tuning series of experiments, convergence ratios will be in the range of 10–15, slightly higher than current convergence ratios for Nova. The sensitivity of the implosion image to symmetry is proportional to the convergence ratio. In present Nova work, instruments easily sense $\sim$2% in asymmetry (with 5 μm spatial resolution in the imaging systems). A convergence ratio of about 15 would be adequate on NIF for confirming asymmetry $<$1%.

The requirements for temporal resolution are similar to those on Nova, i.e., 80–100 ps. To adequately measure the symmetry signature of imploded cores, two x-ray imaging views along and orthogonal to the hohlraum axis are necessary. Equatorial and polar views are designated for this diagnostic.

The gated x-ray imagers require the pinholes to be close to the target. Diagnostics on the NIF with 50 times more energy than Nova must be placed about seven times farther away from the target, i.e., 20 cm, to have incident x-ray flux similar to that on Nova. However, diffraction puts a limit on target-pinhole distance. The optimum pinhole diameter is given by

$$d=\frac{a^2}{4\lambda}\left[1+\frac{1}{m}\right], \tag{1}$$

where d=pinhole diameter that, in the present approximation, is equivalent to the resolution, a=distance from the pinhole to the target, m=system magnification, and λ=wavelength of the x rays being measured.

For the hohlraum tuning campaign, an x-ray energy 8–9 keV is required. At Nova, this imaging energy is usually in the 3–4 keV range. At 9 keV, the instrument can operate at 10 cm and still achieve about 7 μm resolution. A variance of 10 cm in operating distance causes significant questions with respect to parameters such as debris and ablation.

The detector will utilize stripline-gated microchannel plates. To ensure a larger field of view and more channels for each instrument, a 2×2 array of microchannel plates will be housed in each detector. Development work is being pursued to increase the spatial resolution.[11] The image from the back of the P-11 phosphor screen will be relayed to a CCD camera, which outputs image data to a remote, data-acquisition computer.

This diagnostic is a DIM-based system. A redundant alignment concept is proposed that consists of two separate alignment systems. The first is a manual system that requires an opposing port and is very similar to the system now employed on the Nova GXI. To achieve a higher alignment accuracy, an autocollimating telescope and fiducials on the instrument face will be used. The second system is self-contained on the instrument, does not require an opposing port, and has an added benefit of providing remote control. The first system will be used for initial alignments.

F. Filter-fluorescer diagnostic system

The purpose of the filter-fluorescer diagnostic system (FFLEX) is to measure absolute, time-integrated, high-energy x-ray spectra from laser irradiated targets to aid in determining preheat levels.[4] System channel coverage is from 5 to 300 keV using 20 absolutely calibrated channels that are 1–10-keV-wide for x-ray energies $<$100 and $\sim$100 keV wide for x-ray energies $>$100 keV.

The principle of the FFLEX can be illustrated by the example of the lead-gold response channel of this instrument. The diagnostic operates by collimating x rays from the laser-irradiated target and then passing them through a prefilter. In this example, the lead prefilter used has a K-edge at 88 keV. This filter will transmit x rays below 88 keV. These x rays are then made incident on a gold fluorescer foil which has its K-edge at 80 keV. The x rays below 80 keV, which were passed by the lead filter, do not excite the fluorescent K-lines in gold. X rays just above 88 keV are attenuated by the lead filter. Therefore, the primary response or production of fluorescent K-lines in the gold is by the x rays between 80 and 88 keV. There is still a response of the detector channel to x rays well above the prefilter K-edge, but, compared to a single filtered channel, its contribution to the signal has been significantly reduced.

The fluorescer in this experiment significantly reduces the x-ray flux that reaches the detector. It produces the fluorescent x rays, but it also produces scattering of x rays and fluorescence from L and higher shells in the material. To reject these higher-shell fluorescent x rays and the scattered x rays, a postfilter is typically used that has very high transmission for the fluorescent K-lines, but very low transmission for the scattered x rays and the fluorescent x rays from the higher-level shells.

X-ray detectors consist of NaI or plastic fluor scintillators and photomultiplier tubes. The output from each detector is shaped, gated, and integrated to give a single charge from each channel. The time-integrated spectrum is unfolded from these data, taking into account the energy dependence of the channel responses.

Fast shutters will be located in the line-of-sight (LOS) just upstream of the filters to protect the filters, fluorescers, and sensitive detector components from debris. On high yield shots, the LOS will be valved off and a neutron shield inserted behind the valve to prevent activation.

IV. CAPSULE PERFORMANCE DIAGNOSTICS

A. Total neutron yield detector system

The purpose of the total neutron yield detector system (YN) is to measure the total neutron yield in the range from 5×10^{11} to 5×10^{20} neutrons.[4,12] This diagnostic can be easily modified to extend the measurable range down to about 5×10^{8} (or to about 1×10^{7} with a considerable sacrifice in accuracy). If necessary, it could also be modified to measure yields up to about 10^{22}. The diagnostic will be fielded at four locations equally spaced around the target chamber near the equator to provide corroborative measurements of the yield.

This diagnostic is based on nuclear activation. The DT fusion neutrons drive the following reactions in indium and copper:

$$^{115}\mathrm{In}(n,2n)^{114m}\mathrm{In}, \tag{2}$$

$$^{113}\mathrm{In}(n,2n)^{112m}\mathrm{In}, \tag{3}$$

$$^{63}\mathrm{Cu}(n,2n)^{62}\mathrm{Cu}. \tag{4}$$

All three reactions should be used to provide corroborative measurements. The detector systems will be carefully calibrated to provide ''calibration factors'' that will relate the measured ^{114m}In, ^{112m}In, and ^{62}Cu activities to the total neutron yield that induced the activities in the samples. DD fusion neutrons can be measured using the ^{115}In (n,n') ^{115m}In reaction.

These diagnostics can be made more sensitive by moving the samples closer to the target or less sensitive by moving them farther away. At very low yields, one can cross calibrate with a scintillation detector and routinely use the scintillator for low-yield measurements.

Indium and copper activation samples will be 2.5 cm in diameter and have masses ranging from 1 to 50 g each. The indium activities will be measured by counting the gamma rays emitted. This will require two high-purity, 30% efficient germanium detectors. The copper activities will be measured by counting the positrons emitted. To make these measurements will require four, 15 cm$\times$7 cm NaI gamma–gamma coincidence systems.

Two to six samples will be held in a plastic transport capsule (rabbit) that is 9.5-cm-long and 3.8 cm in diameter. The plastic capsules will be housed in rabbit transport housings. Compressed air will force the rabbits back through the transport tubes to the counting laboratory. These systems are routinely used at Sandia at distances of about 60 m and should work at much longer distances, but the range should be investigated before siting the counting laboratory at distance much greater than this.

The only protection necessary is that the innermost 20 cm of tubing must be lined with 3 mm of cadmium to absorb some of the thermal neutrons present. Thermal neutrons can undergo reactions that lead to products that will interfere with the desired measurements.

The data from the two germanium detectors and four NaI gamma-gamma coincidence detectors will be collected, stored, and analyzed using three PC-based data acquisition systems. These systems will be independent of the main data-acquisition system, but, will require a trigger pulse at the time of the shot to provide a $t=0$ starting point for the counting systems.

B. Neutron time-of-flight detector system

The neutron time-of-flight (NTOF) diagnostic for NIF is intended to measure the energy broadening of either DD or DT neutrons over a yield range from 10^{8} to 10^{15}.[4] Three detectors are proposed, one located just outside the vacuum vessel wall from 5 to 6 m from the target, one located between 12 and 20 m from the target, and one located about 40 m from the target along the generic neutron flight path. The detectors will provide a quick neutron yield measurement and also measure the reaction-weighted ion temperature of the fuel. As long as the detector is far enough away from the source, the spread in the arrival time of the neutrons corresponds to the spread in the initial velocity of the neutrons caused by the ion temperature. Therefore, the ion temperature is obtained from the NTOF spread by

$$T_i=(c_1 w/d)^2, \tag{5}$$

where T_i is the ion temperature in keV, w is the full width at half-maximum (FWHM) of the neutron time distribution at the detector in ns, d is the neutron flight path in m, and c_1 is 1.30 for 2.45 MeV DD neutrons and 8.20 for 14 MeV DT neutrons.[4] For a given temperature and distance, the DD neutron time spread will be more than 6 times larger than the DT neutron time spread, and the yield will be around 100 times smaller for the same type of DT target. As a result, DD neutrons will typically be measured using the 6 m detector, while DT neutrons will typically be measured using the 20 m detector.

The detectors consist of fast plastic scintillators, such as quenched BC422, coupled to fast photodetectors. The signal durations are short, tens of ns at most, so a microchannel plate photomultiplier tube (MCP-PMT) is the best choice. Signal levels can be adjusted over a wide range by changing the high voltage applied to the detector.

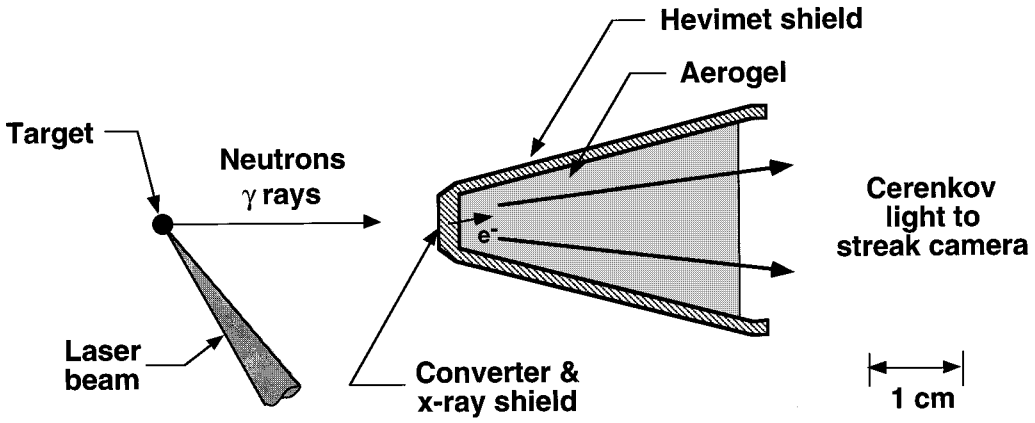

FIG. 6. A schematic of the Cerenkov detector arrangement for reaction history measurements.

C. Neutron imaging system

ICF target-core configuration measurements have relied almost entirely on x-ray imaging. The imploded targets used on the NIF will reach substantially higher areal densities than present Nova targets. As a result, x-ray imaging techniques will eventually fail as the photon yield becomes intractably small. Neutron imaging (NI) offers an alternative measurement that is almost completely insensitive to the target areal density. Moreover, the thick neutron aperture can be made sufficiently rugged to withstand the hostile environment of the NIF target chamber during high-yield experiments.

Either a penumbral or annular coded aperture similar to the present Nova neutron microscope should be used to achieve high resolution and good sensitivity.[13] The aperture is mounted rather close to the target, producing an image on a high-efficiency, low-resolution detector operating at high magnification. This provides the highest possible sensitivity for nonigniting targets. The aperture would be a tapered hole or annulus formed in a gold cylinder by timed-draw electroplating methods and be positioned 10 cm from the target. This puts the ''focal point'' of the aperture approximately 14 cm from the target: A magnification of 240 would be required to achieve the spatial resolution of 10 μm, which would limit the aperture field-of-view to 300 μm. To produce a legible image, this instrument would require yields of 10^{12} DT neutrons, or 10^{13} DD neutrons. The aperture would be supported with its front face approximately 10 cm from the target by a DIM or similar manipulator. The detector will be located approximately 34 m from the target.

The neutron detector would be based on organic scintillator fibers. A 30-cm-square array would consist of 90 000 1-mm-square scintillators. The large image would be segmented, reduced, and intensified using a fiber-optically coupled CCD readout scheme similar to the present Nova neutron detector.

Because of the limited field-of-view of the neutron aperture, a high-precision (± 5 μm) alignment system is required. An alignment laser beam must be injected from an opposing port to establish a straight-line reference between the target position and the detector. The aperture can then be pointed and centered to this reference.

D. Fusion reaction history diagnostics

Fusion reaction rate provides information about compressed fuel core in an ICF target. Two quantities are of interest in performing these measurements. The first is bang time which is defined as that time interval between the 50% rise-time of on target laser power and the time of peak thermonuclear emission from the target. The other quantity of interest is the time history of the thermonuclear emission from the target. Both of these quantities depend on detailed target hydrodynamics, plasma conditions, and are a sensitive indicator of modeling accuracy.

For NIF, gamma-ray methods are being investigated as a replacement for neutron-based fusion history measurements.[14] At Nova, burn-history measurements are routinely made by detecting the arrival times of nearly monoenergetic fusion neutrons with a fast (25 ps) detector relatively close (2–20 cm) to the target. The recorded neutron time distribution at the detector is the fusion burn history delayed by the neutron time of flight. Doppler-induced broadening of the neutron energy spectra causes a spread in the temporal signal at the detector that is proportional to the target-to-detector distance and the square root of the plasma ion temperature. For a 1 keV plasma, a 20 ps spread is reached at 16 cm for DT neutrons and 6 cm for DD neutrons. At NIF, it is unlikely that a detector can be placed close enough to a target to make a direct neutron measurement with resolutions approaching 30 ps. Indeed, for high energy NIF targets which require detectors be placed at the chamber wall 5 m away, Doppler-induced broadening will be 610–1930 ps for 1 to 10 keV ion temperatures.

Besides neutrons, deuterium–tritium fusion reactions occasionally produce 16.7 MeV gamma rays. Since gamma ray temporal distribution at a point distant from a target (point source) is unaffected by either distance or temperature, it may be possible to use them for fusion history measurements. The biggest challenge is the low branching ratio of 5×10^{-5} for gamma production. Use of gamma rays for fusion history measurements requires the development a fast, sensitive gamma-ray detector.

One possible detection technique that is currently being investigated for this application, is a two-stage gamma-ray-

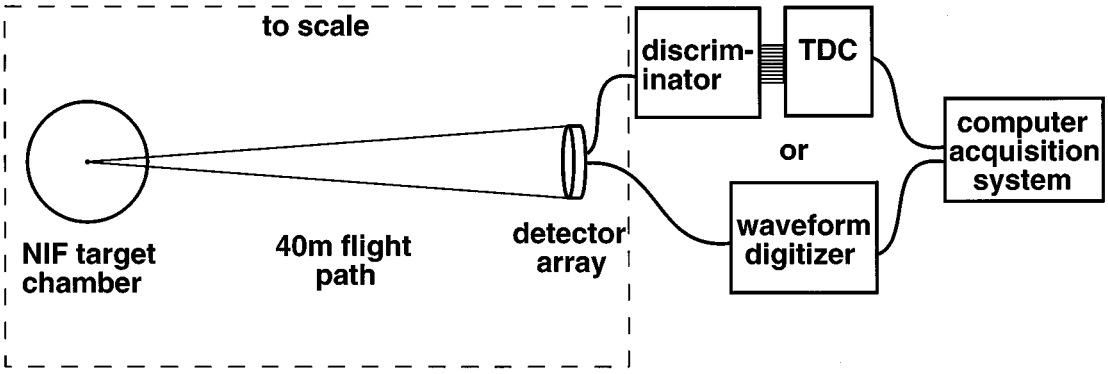

FIG. 7. A conceptual drawing of the NIF tertiary neutron diagnostic.

to-light converter shown in Fig. 6. In the first converter stage, target gamma rays interact via pair production with a high-Z material. The resulting relativistic electrons and positrons travel through a second material such as an aerogel foam where they produce Cerenkov light. The material used for the second converter stage sets a threshold for the minimum gamma ray energy detectable and determines the amount of Cerenkov light produced.

This technique has been used to detect fusion gamma rays in a set of preliminary experiments at Nova. For these experiments, the fast plastic scintillator in the nose cone of the Nova (neutron-based) burn history detector was replaced with an aerogel foam to produce a two stage gamma converter. The first converter stage is the 3-mm-thick Hevimet (90% tungsten) cone which surrounds the second stage aerogel foam. An $f/2$ optic relays light from the nose cone to a high-speed streak camera for recording. With this arrangement, the ability to detect fusion gamma rays has been demonstrated. Signals recorded with the nose cone at different target to detector distances (2, 3, and 4 cm) show different temporal separation between observed gamma ray and neutron signals. When the Hevimet nose cone is replaced with an aluminum one, the x-ray signal goes down by at least a factor of 20 indicating the gamma signal depends strongly on the high-Z converter. Null experiments with the aerogel foam removed show that the neutron signal is caused by neutron interactions in our $f/2$ optic and that there is almost no signal produced by neutrons interacting in the aerogel foam.

E. Tertiary neutron spectroscopy diagnostic system

Fuel areal density $\langle \rho R \rangle$ is an important fundamental ICF parameter that has historically been measured by a variety of techniques. In recent years, the fuel areal density of implosions of interest has been steadily increasing and has therefore required that new techniques be developed for its measurement. Since neutrons can escape from the core of even the largest targets, experimental measurements of fuel areal density have become primarily neutron based.

For today's experiments at Nova, the measurement of secondary DT neutrons produced in an initially pure deuterium fuel has become the primary diagnostic technique for the determination of fuel areal density.[15] Because of triton slowing with increasing $\langle \rho R \rangle$, this method fails at $\langle \rho R \rangle$ values that approach 20–30 mg/cm^2. On NIF, where the $\langle \rho R \rangle$ values are much larger, tertiary neutrons must be used to measure fuel $\langle \rho R \rangle$. In this technique, a chain of three reactions are used. These reactions are

$$d + t \rightarrow \alpha(3.5\ \text{MeV}) + n(14.1\ \text{MeV}), \tag{6}$$

$$n(14.1\ \text{MeV}) + d \rightarrow n' + d'(0\text{–}12.5\ \text{MeV}), \tag{7}$$

$$d'(0\text{-}12.5\ \text{MeV}) + t \rightarrow \alpha + n(12\text{–}30.1\ \text{MeV}). \tag{8}$$

The sequence of events in these three reactions are that the primary 14.1 MeV neutron from reaction (1) elastically scatters with fuel deuteron to produce a fast deuteron. This fast deuteron then interacts with a fuel triton to produce a tertiary neutron that has an energy in the range of 12 to 30.1 MeV. For negligible ion slowing (no energy dependent cross-section effects), the number of tertiary neutrons produced is proportional to $\langle \rho R \rangle^2$ for areal fuel densities from zero to beyond 1 g/cm^2. The faction of tertiaries to all neutrons for NIF target conditions is of order 2×10^{-4}. Tertiary neutrons produced at energies $>\sim$28 MeV must come from a situation in which all of the interactions are aligned in one direction. This fact can be exploited to give directional information on $\langle \rho R \rangle$ as a function of angle by fielding an array of detectors located at different angular positions around the target.

A conceptual design of a tertiary neutron diagnostic for NIF is shown in Fig. 7. In this design, a neutron detector array similar to the array fielded on Nova would be located at 40 m from the target. The output of each detector in the array would either be processed through a conventional discrimator and time to digital converter as is now done on Nova or through a waveform digitizer. The final detector design will depend on technological advances in the next five years.

F. Tertiary proton spectroscopy diagnostic system

Tertiary protons with birth energies from $\sim$27 to 30.8 MeV will provide important information about implosion symmetry and areal fuel densities on the NIF.[16] High-energy tertiary protons are generated in a 3-step process starting with the primary fusion between deuterium (d) and tritium (t) ions

$$d + t \rightarrow \alpha(3.5\ \text{MeV}) + n(14.1\ \text{MeV}), \tag{9}$$

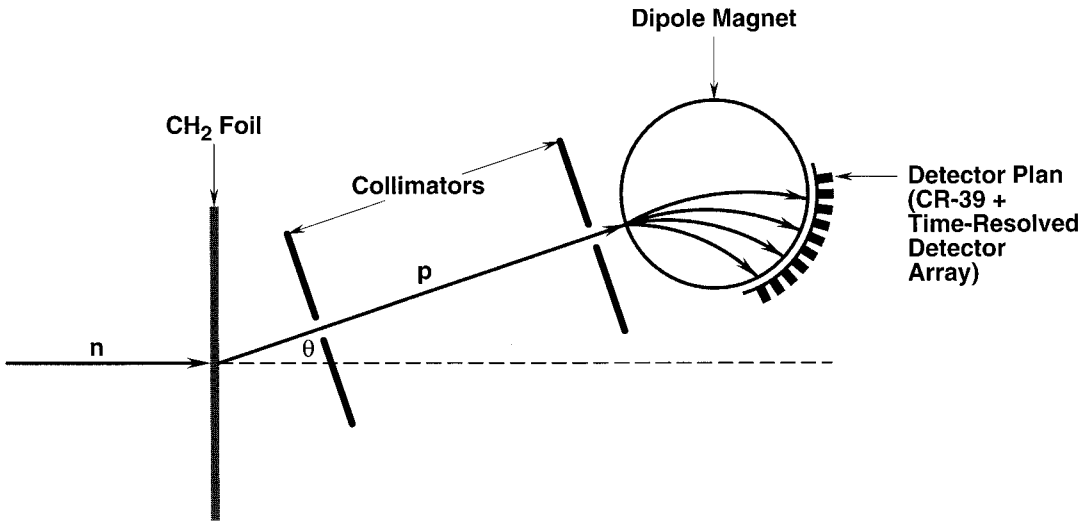

FIG. 8. A conceptual drawing of the $n-p$ recoil neutron diagnostic.

where the α particles are responsible, because of their short range, for propagating the burn outwards from the core ''sparkplug'' into the dense fuel region. The second step involves the 14.1 MeV neutron elastically scattering off a deuteron:

$$n(14.1\ \text{MeV})+d\rightarrow n'+d(11-12.5\ \text{MeV}). \tag{10}$$

11 (12.5 MeV) corresponds to a collision in which the deuteron scatters at 20° (0°) with respect to the incident neutron direction. Because the differential cross section is strongly peaked in the forward direction, about 13% of the reactions result in deuteron energies at or above 11 MeV. The third and final step involves these very energetic deuterons fusing with ^{3}He, with tertiaries being emitted within 30° (20°) of the forward direction:

$$d(11-12.5\ \text{MeV})+{}^3\text{He}\rightarrow\alpha+p[27.6(28)-30.8\ \text{MeV}]. \tag{11}$$

Because this differential cross section is also strongly forward peaked, about 17% (12)% of all tertiary protons are emitted with energies at or above 27.6 (28) MeV. This reaction requires the presence of ^{3}He, which is intentionally introduced into the capsule during fabrication.

One possible realization of the tertiary proton diagnostic on NIF would be to use multiple proton magnetic spectrographs simultaneously viewing the implosion from various angles, differences in their spectra being related to variations in fuel $\langle\rho R\rangle$ and electron temperature along the different line-of-sights. The interest in fielding the diagnostic in this manner is because 2D radiation hydrodynamic calculations for ignited NIF capsules indicate that pole-to-waist angular variations in the cryogenic fuel $\langle\rho R\rangle$ can vary by as much as 40% from 1D density profile calculations.

G. Proton recoil technique for high yield neutron measurements

The high level of thermonuclear output of an NIF target open up the possibility of several new classes of neutron diagnostics.[17,18] These diagnostics are based on the measurement of proton recoils from the interaction of 2.45 and 14.1 MeV neutrons in thin CH_2 foils (of order 10-mg/cm^2-thick). The diagnostics would operate by detecting the proton recoils at near forward angles in either time-integrated detectors or time-resolved current mode detectors. The protons may be energy resolved using range filters or by magnetic analysis in a simple dipole magnet spectrograph. Such a magnetic spectrograph is conceptually shown in Fig. 8 in which protons scattered from a CH foil are collimated and magnetically analyzed. An attractive feature of these types of neutron diagnostics is that the neutron energy E_n and the proton energy E_p at an angle θ relative to the original neutron direction is simply related by $E_p=E_n\cos^2(\theta)$. Additionally, the elastic n-p cross section is very well known at both 2.45 and 14.1 MeV. For neutron yields approaching ignition on the NIF facility, these two advantages largely offset the insensitivity of the technique. These diagnostic techniques offer a very clean measurement of neutron yield that can be almost entirely free of scattered neutron backgrounds. At higher neutron yields, measurements of time-resolved ion temperature and reaction burn time become possible. A direct analog of these diagnostics is the Rutherford ion pinhole camera and Rutherford magnetic analyzer diagnostics successfully used in intense ion beam measurements. These diagnostics are based on the detection of elastically scattered protons or higher-Z ions that are Rutherford scattered by thin gold foils.[19] Additionally, Kallne has proposed a similar arrangement for use on tokamaks.[20]

V. SUMMARY

A review of recent progress on the design of a diagnostic system proposed for ignition target experiments on the National Ignition Facility (NIF) has been presented. Diagnostics comprising this system fall into three classes: laser characterization, hohlraum characterization, and capsule performance. These three classes of diagnostics can be further categorized into ''facility-provided'' and ''experiment-specific''

diagnostics. The operating principles of each diagnostic were described.

ACKNOWLEDGMENT

This work was supported by the U. S. Department of Energy under Contract No. DE-AC04-94AL85000.

[1] S. W. Haan, S. M. Pollaine, J. D. Lindl, L. J. Suter, R. L. Berger, L. V. Powers, W. E. Alley, P. A. Amendt, J. A. Futterman, W. K. Levedahl, M. D. Rosen, D. P. Rowley, R. A. Sacks, A. I. Shestakov, G. L. Strobel, M. Tabak, S. V. Weber, G. B. Zimmerman, W. J. Krauser, D. C. Wilson, S. Coggeshall, D. B. Harris, N. M. Hoffman, and B. H. Wilde, Phys. Plasmas **2**, 2480 (1995).
[2] J. D. Kilkenny, Rev. Sci. Instrum. **63**, 4688 (1992).
[3] O. L. Landen, R. A. Lerche, R. G. Hay, B. A. Hammel, D. Kalantar, and M. D. Cable, Rev. Sci. Instrum. **66**, 788 (1995).
[4] J. D. Kilkenny, M. D. Cable, C. A. Clower, B. A. Hammel, V. P. Karpenko, R. L. Kauffman, H. N. Kornblum, B. J. MacGowan, W. Olson, T. J. Orzechowski, D. W. Phillion, G. L. Tietbohl, B. Chrien, B. Failor, A. Hauer, R. Hockaday, J. Oertel, R. Watt, C. Ruiz, G. Cooper, D. Hebron, R. Leeper, J. Porter, and J. Knauer, Rev. Sci. Instrum. **66**, 288 (1995).
[5] R. K. Kirkwood, C. A. Back, S. H. Glenzer, B. J. MacGowan, D. S. Montgomery, and J. D. Moody, Rev. Sci. Instrum., these proceedings.
[6] B. MacGowan *et al.*, LLNL ICF Quarterly Report No. 5, 305, UCRL-LR-1015821-95-4, 1995 (unpublished).
[7] M. D. Wilke, J. C. Fernandez, R. R. Berggren, D. Montgomery, J. Faulkner, L. Looney, and J. Jimerson, Rev. Sci. Instrum., these proceedings.
[8] H. N. Kornblum, R. L. Kauffman, and J. A. Smith, Rev. Sci. Instrum. **57**, 2179 (1986).
[9] J. L. Porter, Rev. Sci. Instrum., these proceedings.
[10] R. L. Kauffman, L. J. Suter, C. B. Darrow, J. D. Kilkenny, H. N. Kornblum, D. S. Montgomery, D. W. Phillion, M. D. Rosen, A. R. Theissen, R. J. Wallace, and F. Ze, Phys. Rev. Lett. **73**, 2320 (1994).
[11] P. M. Bell, J. D. Kilkenny, O. L. Landen, R. L. Hanks, and D. K. Bradley, Rev. Sci. Instrum. **63**, 5072 (1992).
[12] C. W. Barnes, Rev. Sci. Instrum., these proceedings.
[13] R. A. Lerche, D. Ress, R. J. Ellis, S. M. Lane, and K. N. Nugent, Laser Particle Beams **9**, 99 (1991).
[14] R. A. Lerche, D. W. Phillion, and G. L. Tietbohl, Rev. Sci. Instrum. **66**, 933 (1995).
[15] M. B. Nelson and M. D. Cable, Rev. Sci. Instrum. **63**, 4874 (1992).
[16] R. D. Petrasso, C. K. Li, M. D. Cable, S. M. Pollaine, S. W. Haan, T. P. Bernat, J. D. Kilkenny, S. Cremer, J. P. Knauer, C. P. Verdon, and R. L. Kremens, Phys. Rev. Lett. (submitted).
[17] R. J. Leeper, C. L. Ruiz, and G. W. Cooper, Conference Record, 22nd IEEE International Conference On Plasma Science, Madison, Wisconsin, June 5–8, 1995 (unpublished), p. 153.
[18] T. J. Murphy, Conference Record, 22nd IEEE International Conference On Plasma Science, Madison, Wisconsin, June 5–8, 1995 (unpublished), p. 152.
[19] R. J. Leeper, W. A. Stygar, R. P. Kensek, J. R. Lee, D. J. Johnson, T. R. Lockner, J. Maenchen, D. E. Hebron, and D. F. Wenger, Rev. Sci. Instrum. **59**, 1700 (1988).
[20] J. Kallne and H. Enge, Nucl. Instrum. Methods Phys. Res. A **311**, 595 (1992).